Published in final edited form as:
Dev Biol. 2014 November 1; 395(1): 29–37. doi:10.1016/j.ydbio.2014.09.001.

Epithelial sheet movement requires the cooperation of c-Jun and MAP3K1

Qinghang Meng[#1], **Maureen Mongan**[#1], **Jingjing Wang**[1], **Xiaofang Tang**[2], **Jinling Zhang**[1], **Winston Kao**[3], and **Ying Xia**[1,3,4]

[1]Department of Environmental Health, University of Cincinnati, College of Medicine

[2]Division of Developmental Biology, Cincinnati Children's Hospital Medical Center

[3]Department of Ophthalmology, University of Cincinnati, College of Medicine

[#] These authors contributed equally to this work.

Abstract

Epithelial sheet movement is an essential morphogenetic process during mouse embryonic eyelid closure in which Mitogen-Activated Protein 3 Kinase 1 (MAP3K1) and c-Jun play a critical role. Here we show that MAP3K1 associates with the cytoskeleton, activates Jun N-terminal kinase (JNK) and actin polymerization, and promotes the eyelid inferior epithelial cell elongation and epithelium protrusion. Following epithelium protrusion, c-Jun begins to express and acts to promote ERK phosphorylation and migration of the protruding epithelial cells. Homozygous deletion of either gene causes defective eyelid closure, but non-allelic non-complementation does not occur between *Map3k1* and *c-Jun* and the double heterozygotes have normal eyelid closure. Results from this study suggest that MAP3K1 and c-Jun signal through distinct temporal-spatial pathways and that productive epithelium movement for eyelid closure requires the consecutive action of MAP3K1-dependent cytoskeleton reorganization followed by c-Jun-mediated migration.

Keywords

MAP3K1; c-Jun; embryonic eyelid closure

INTRODUCTION

Coordinated migration of epithelial sheets is a key biological process in developmental morphogenesis and adult tissue homeostasis (Gumbiner, 1992). Studies in model systems, including wound healing, gastrulation and eyelid closure, provide important insights into the mechanisms of epithelial morphogenesis. Eyelid closure is an essential step of mammalian

[4]To whom correspondence should be addressed: Ying Xia, Ph.D., Department of Environmental Health, University of Cincinnati, College of Medicine, 123 East Shields Street, Cincinnati, Ohio 45267-0056, ying.xia@uc.edu, Phone: 513-558-0371 .

development and has been best characterized in mice. Mouse eyelid starts to form around embryonic day 11.5 (E11.5) with the invagination of the ocular surface ectoderm adjacent to the eye globe. The epithelium at the eyelid leading edge elongates and migrates centripetally and ultimately fuses between E15.5 and E16.5 (Findlater et al., 1993;Harris and McLeod, 1982). The eyelid remains closed between E16.5 and postnatal day 12-14. About two weeks after birth, and coinciding with the maturation of cornea and retina, cells at the eyelid fusion junction undergo desquamation and apoptosis. This results in fission of the upper and lower eyelids (Findlater et al., 1993;Mohamed et al., 2003).

Being the last major morphogenetic event in embryogenesis, eyelid closure is not required for embryo survival, but its failure is associated with aberrant development of cornea and eyelid muscles. Failure of eyelid closure occurs in more than 138 genetic mutant strains (http://www.informatics.jax.org/), resulting in an easily identifiable eye-open-at-birth (EOB) phenotype. The plethora mutations that confer the EOB phenotype underscore the complexity of the genetic control over eyelid morphogenesis and the ample possibility of genetic lesions causing congenital eye defects. The EOB strains are also valuable resources to investigate the cellular and molecular mechanisms underlying epithelial sheet migration and genetic basis of developmental diseases.

One of the genes that control eyelid morphogenesis is *Map3k1*, coding for the mitogen-activated protein 3 kinase 1. Inactivation of *Map3k1* in mice causes the EOB phenotype with 100% penetrance (Yujiri et al., 1998;Zhang et al., 2003). MAP3K1 is a member of the MAP3K superfamily, responsible for activation of the MAP2K-MAPK cascades (Uhlik et al., 2004). In the developing eyelid, MAP3K1 is expressed abundantly in the epithelial cells, where it is required for activation of the Jun N-terminal kinases (JNKs) MAPKs (Zhang et al., 2003). Various genetic and molecular analyses have shown that eyelid closure is dependent, at least partially, on signals transmitted through the MAP3K1-JNK axis (Takatori et al., 2008;Weston et al., 2003;Zhang et al., 2003).

Signals transmitted through this axis lead to the phosphorylation of c-Jun on serine residues 63 and 73 by JNK (Derijard et al., 1994;Hibi et al., 1993). In the developing eyelid epithelium, c-Jun phosphorylation is abundant in wild type fetuses, and is indeed markedly decreased in *Map3k1*$^{-/-}$ and *Map3k1*$^{+/-}$ *Jnk1*$^{-/-}$ fetuses (Geh et al., 2011;Takatori et al., 2008). While the MAP3K1-JNK axis leads to c-Jun phosphorylation, phosphorylation of c-Jun may not be required for eyelid closure. Transgenic mice, harboring a knock-in c-Jun mutant with serines 63 and 73 replaced by alanines [c-Jun (AA)] display normal eyelid development even though the c-Jun mutant can no longer be phosphorylated by JNK (Behrens et al., 1999). These observations raise the possibility that the MAP3K1-JNK cascade regulates eyelid morphogenesis through downstream targets other than the phosphorylation of c-Jun. Paradoxically, although c-Jun phosphorylation is dispensable, c-Jun expression in the epithelial cells is essential for eyelid closure, since mice with conditional *c-Jun* gene ablation in keratinocytes (*c-Jun-skin*- null) have normal skin architecture, but display an EOB phenotype (Li et al., 2003;Zenz et al., 2003).

In addition to the EOB phenotype, both the *Map3k1*-null mice and the *c-Jun-skin*-null mice have delayed epidermal wound healing; epithelial cells derived from these mice display

impaired migration (Deng et al., 2006;Li et al., 2003). Defective epithelial cell migration appears to be the common cause of the eyelid closure defect in these mutants; however, how MAP3K1 and c-Jun coordinate in the regulation of epithelial sheet movement has not been fully characterized. We have used genetic, molecular, histological and imaging approaches to investigate the role of MAP3K1 and c-Jun in eyelid morphogenesis. We find that MAP3K1 and c-Jun have different patterns of temporal-spatial expression and regulate distinct cellular activities in the developing eyelids. Homozygous mutation of either gene results in defective eyelid closure, but the compound double heterozygous mice do not manifest this defect. Hence, as far as embryonic eyelid closure is concerned, MAP3K1 and c-Jun seem to operate on independent parallel pathways to regulate epithelial sheet movement.

MATERIALS AND METHODS

Mouse colonies, reagents and antibodies

The *Map3k1*$^{\Delta/\Delta KD}$ and *Le-cre* mice were described before (Geh et al., 2011;Zhang et al., 2003). The *c-Jun*^{F} mice were generous gifts from Dr. Randall Johnson (University of California, San Diego, USA) (Li et al., 2003). Mice mating and handling used standard protocols, approved by the Institutional Animal Care and Use Committee at the University of Cincinnati.

The antibodies for c-Jun, JNK, γ-tubulin, and β-Actin were from Santa Cruz Biotechnology (Santa Cruz, CA, USA), anti-phospho-JNK was from Promega (Medison, WI, USA), anti-p-c-Jun, p-ERK and paxillin were from Millipore (Billerica, MA, USA), anti-β-catenin was from BD Biosciences Pharmingen (San Jose, CA, USA), anti-HA was from Covance (Dedham, MA, USA), and anti-keratin 14 was from Sigma (St. Louis, MO, USA). The anti-MAP3K1 was raised in rabbits against bacterially expressed fusion protein GST-hMAP3K1 (aa1026-1190) as described previously (Xia et al., 2000). Colchicine and cytochalasin D were from Calbiochem (Billerica, MA, USA), X-gal was from Gold Biotechnology (St. Louis, MO, USA), and the 4′,6-diamidino-2-phenylindole (DAPI), Harris Hematoxylin solution and alcoholic Eosin Y solution were from Sigma (St. Louis, MO, USA). The Alexa Fluor-conjugated secondary antibodies and phalloidin, lipofectamine plus, random hexamer primers, and reverse transcription reagents were from Invitrogen (Grand Island, NY, USA).

Cell culture, plasmids and transient transfection

The Human Embryonic Kidney 293 (HEK 293), the human breast cancer cell line MCF-7, the immortal human keratinocyte line HaCaT, and the cervical cancer epithelial cell HeLa were originally from the American Type Culture Collection (ATCC). The wild type and *Map3k1*$^{\Delta/\Delta KD}$ fibroblasts were described before (Geh et al., 2011). The cells were maintained in Dulbecco's modified Eagle's medium (DMEM) with 10% fetal bovine serum (FBS) from Cellgro. Transient transfection was performed using lipofectamine-plus following the protocols provided by the manufacturer.

Histology, β-galactosidase staining, immunostaining and imaging

Whole mount X-gal staining was carried out as described before (Mongan et al., 2008). For histology and immunohistochemistry, embryos' heads were fixed in 4% paraformaldehyde at 4°C overnight. Tissues were embedded in either paraffin or OCT and frozen. Tissue sections were processed using standard protocols, followed by either Hematoxylin/Eosin or immunostaining. Transfected HeLa cells on 12-mm glass cover slips were fixed with 4% formaldehyde, followed by permeablization and immunostaining. Immunostaining was done by using specific antibodies plus Alexa Fluor dye-conjugated secondary antibodies, Alexa Fluor dyeconjugated Phalloidin to label F-actin, and Hoechst to stain nuclei. Images were captured using a Leica MZ16 FA dissecting microscope, Zeiss Axio microscope equipped with an AxioCam ERc5s and Zeiss Axioplan 2 imaging fluorescence microscope, or Nikon A1R si inverted single photon laser scanning microscope.

Measurement of cell elongation index

The tissue sections of E15.5 fetuses were processed for H&E staining and the developing eyelids were photographed. Ten sections of each head and 3 heads of each genotype were examined. The length and width of the nuclei were measured using AxioVision (Zeiss). Cell elongation index was calculated by dividing the length by the width.

Isolation of Triton X-100 resistance fractions and Western blotting

The Triton X-100 insoluble fraction was isolated as previously described (Posern et al., 2004). Briefly, cells were lysed in Triton lysis buffer (50 mM NaCl, 1 mM EDTA, 0.5% Triton X-100, 20 mM HEPES, pH 7.9), and the lysates were subjected to centrifugation at 100,000 g for 1.5 h. The supernatants contained the triton soluble fractions, whereas the pellets contained the triton insoluble fractions, enriched for cytoskeleton associated proteins. The pellets were resuspended in Triton lysis buffer and dispersed by sonication. Total cell lysates were prepared in RIPA buffer containing 50 mM Tris-HCl (pH7.5), 0.1% Nonidet-P40, 120 mM NaCl, 1mM EDTA, 6 mM EGTA, 20 mM NaF, 1 mM NaPyrophosphate and protease inhibitors and collecting the supernatants after centrifugation at 14,000 × g for 5 min. Fifty to one hundred micrograms of fractionated or total lysates were mixed with SDS-PAGE loading buffer, separated by SDS-PAGE and detected by immunoblotting with appropriate antibodies.

RNA isolation, reverse transcription and real-time quantitative polymerase chain reaction (PCR)

RNA was isolated from cultured cells using Tri-reagent (Molecular Research Center) and purified by RNeasy Mini Kit (QIAGEN, Germantown, MD, USA). Reverse transcription was performed using SuperScript III RNase H-reverse transcriptase (Invitrogen, Grand Island, NY, USA). Real time quantitative RT-PCR was performed with a mixture containing Power SYBR Master Mix (Agilent Technology, Santa Clara, CA, USA) and 2.5 μM of each forward and reverse primer for target mRNA. The sequences of primers used for mRNA quantification can be found in Supplemental Table S1. Amplification was performed on a MX3000p thermal cycler system with conditions optimized for each target gene primers with efficiency greater than 85%, less than 28 cycles and with randomized plate sample

locations. PCR efficiencies were verified by examination of the corresponding melting curves for each primer pair. Amplification of *Gapdh* cDNA in the same sample was used as an internal control for all PCR amplification reactions. Data, based on triplicate reactions of at least 3 biological samples, were calculated by using the ΔΔCT method, as described (Schnekenburger et al., 2007), where $\Delta\Delta Ct = (Ct^{\text{Gene}} - Ct^{\text{Actin}})_{\text{Exp}} - (Ct^{\text{Gene}} - Ct^{\text{Actin}})_{\text{Control}}$.

Statistical analyses

Statistical comparisons were performed with Student's two-tailed paired *t test*. Values of *P < 0.05, **P < 0.01, and ***P < 0.001 were considered statistically significant.

RESULTS

c-Jun is essential for eyelid closure

To verify the role of c-Jun in eyelid development, we crossed mice homozygous for a floxed *c-Jun* allele (*c-Jun*$^{F/F}$) with *c-Jun*$^{F/F}$/*le-cre* mice, which express Cre recombinase in the ocular surface ectoderm starting on E9.5 (shery-Padan et al., 2000). In the resultant E15 *c-Jun*$^{F/F}$ fetuses, c-Jun positive cells were scattered in the eyelid stroma and epithelium (Fig. 1A). c-Jun expression was low in basal epithelial cells, but was markedly elevated in a group of suprabasal cells located in the eyelid leading edge. The expression of c-Jun appeared to be restricted in the K14-positive epithelial cells, located underneath the K14-negative periderm layer that was shown to be dispensable for eyelid closure (Heller et al., 2014)(Fig. S1). In the *c-Jun*$^{F/F}$/*le-cre* fetuses, c-Jun positive cells were absent in the eyelid epithelium, but were still present in the eyelid stroma, indicating that *c-Jun* was ablated specifically in the eyelid/ocular surface epithelium (OSE). These mice are hereafter referred to as *c-Jun*$^{\Delta/\Delta OSE}$.

The *Jun*$^{\Delta/\Delta OSE}$ fetuses have a normal appearance, but the majority (32 of 38 or 84%) exhibits an EOB phenotype (Fig. 1B). Morphologically, eyelids of the *c-Jun*$^{F/F}$ and *Jun*$^{\Delta/\Delta OSE}$ mice are indistinguishable at E15.5, but become drastically different at E16.5. While the E16.5 *c-Jun*$^{F/F}$ eyelids fuse, covering the corneal surface, the *Jun*$^{\Delta/\Delta OSE}$ eyelids are still widely open (Figs. 1B and 1C). This difference persists throughout the embryonic/fetal phases.

Detailed morphological features indicate that the process of eyelid closure transitions from pre-initiation (E15) to initiation (E15.5) to progression (E16) phases. At E15, the epithelium is a smooth surface in the eyelid leading edge, but at E15.5 it forms a tiny protrusion in the eyelid tip, and at E16 the protrusion extends considerably towards the center of the eye surface (Fig. 1D). The eyelid morphology was identical between wild type and *Jun*$^{\Delta/\Delta OSE}$ fetuses at E15 and E15.5, but was different at E16. In contrast to the wild type E16 fetuses, in which the eyelid epithelium protrusion continues to migrate across the ocular surface, the *Jun*$^{\Delta/\Delta OSE}$ eyelid epithelium fails to move forward. Hence, although c-Jun is not required for the formation of epithelium protrusion, it promotes the continuous extension of the protruding eyelid epithelium.

Genetic inactivation of various components of the EGFR pathway results in the EOB phenotype (Fowler et al., 1995;Hassemer et al., 2010;Miettinen et al., 1995;Mine et al., 2005;Sibilia and Wagner, 1995;Threadgill et al., 1995). The EGFR signaling cascade is a potential target of c-Jun activity, as c-Jun directly regulates the expression of EGFR and its ligand heparin-binding EGF-like growth factor (HB-EGF) (Grose, 2003;Zenz et al., 2003). To evaluate whether c-Jun deletion affected the EGFR signaling in eyelid epithelium, we examined the phosphorylation of ERK, an EGFR regulated downstream event. ERK phosphorylation in the eyelid tip epithelial cells was indeed more abundant in wild type than in $Jun^{\Delta/\Delta OSE}$ fetuses (Fig. 1E). The migration marker, β-catenin dissociation from plasma membrane, was obvious in wild type but less apparent in $Jun^{\Delta/\Delta OSE}$ eyelids (Fig. 1F). These observations suggest that c-Jun promotes eyelid epithelium extension through a mechanism likely to involve EGFR/ERK activation and epithelial cell migration.

MAP3K1 regulates actin polymerization and epithelial cell elongation Map3k1$^{\Delta/\Delta KD}$

mice express a kinase-inactive MAP3K1(N)-β-gal fusion instead of the wild type protein, and like the $Jun^{\Delta/\Delta OSE}$ mice, are also born with an EOB phenotype (Zhang et al., 2003). To characterize the developmental processes regulated by MAP3K1, we examined E15-E16.5 eyelids for morphological features associated with MAP3K1 ablation. All the $Map3k1^{\Delta/\Delta KD}$ eyelids lacked epithelial tip protrusion and kept the morphology of the pre-initiation phase (Fig. 2A). Thus, unlike $c\text{-}Jun^{\Delta/\Delta OSE}$ fetuses that are defective in epithelium extension at the progression phase, $Map3k1^{\Delta/\Delta KD}$ fetuses seem to be defective at the initial phase of lid closure.

To identify the cells in which MAP3K1 is expressed, we examined the eyes of whole mount X-gal stained $Map3k1^{+/\Delta KD}$ fetuses. The β-gal-positive cells were located in the eyelid leading edge at all eyelid closure phases and were particularly enriched in the K14-positive epithelium at the inferior side of the eyelid (Figs. 2B and S1). At the initiation phase of lid closure, strong β-gal expression was accumulated in a small group of cells near the eyelid tip and, at the progression and completion phases, in the epithelial extension and lid fusion junction.

In the wild type fetuses, the inferior epithelial cells near the eyelid tip were elongated, stretching towards the center of the opening; in contrast, these cells did not elongate in the $Map3k1^{\Delta/\Delta KD}$ fetuses and retained a round morphology (Fig. 2C). In fact, the elongation index of wild type and $Map3k1^{+/\Delta KD}$ cells was twice that of $Map3k1^{\Delta/\Delta KD}$ cells (Fig. 2D). Epithelial cell elongation is driven by F-actin re-organization and alignment of stress fibers along the cell axis. In wild type but much less so in $Map3k1^{\Delta/\Delta KD}$ fetuses, F-actin was enriched in inferior cells near the eyelid tip (Figs. 2E and 2F). These *in vivo* data suggest that MAP3K1 regulates actin polymerization and cell elongation for the initiation of eyelid closure.

To verify that MAP3K1 regulates actin polymerization, we used transient expression of HA-tagged wild type (WT) or kinase-inactive mutant (KM) MAP3K1 in HeLa cells, and measured HA expression and F-actin formation. The F-actin in MAP3K1(WT)-positive cells was more abundant than in HA-negative cells and formed stress fibers, but was less abundant and remained as cortical cables in MAP3K1(KM)-expressing cells (Fig. 3A). The

amount of F-actin was significantly increased by expression of MAP3K1(WT) but decreased by expression of MAP3K1(KM) (Fig. 3B), indicating that MAP3K1 activity is required to promote actin polymerization.

HA-MAP3K1 appeared under confocal microscopy as punctated dots, often co-localized along the F-actin fibers (Fig. 3C). To assess whether MAP3K1 might be directly associated with the actin cytoskeleton, we isolated the Triton X-100 insoluble cytoskeletal fraction from HEK 293 cells transfected with HA-MAP3K1(WT) or (KM) expression plasmids. Approximately 6% and 1% of the MAP3K1(WT) and MAP3K1 (KM) proteins, respectively, was present in the Triton-soluble fraction, and more than 90% was present in the Triton-insoluble fraction (Figs. 3D, S2A and S2B). The endogenous MAP3K1 was also detected in the cytoskeleton fraction in various types of cultured cells (Figs. 3E). The expression of endogenous MAP3K1 proteins in the developing eyelids was similar to the pattern detected by X-gal staining (see Fig. 2B) and was more abundant in the inferior epithelium than in the rest of the epithelium (Fig. 3F). Co-localization of MAP3K1 with F-actin fibers could readily be detected in a few cells located near the eyelid leading edge. This observation suggests that MAP3K1 is associated with F-actin *in vivo* in specific eyelid epithelial cells.

The *in vivo* and *in vitro* data together suggest that MAP3K1 is physically associated with the cytoskeleton, where its kinase activity promotes actin polymerization and the elongation of a subset of eyelid suprabasal epithelial cells, leading to the formation of an epithelium protrusion and the initiation of lid closure.

MAP3K1 is required for c-Jun phosphorylation, but not its expression

Expression of c-Jun in the developing epithelium is weak, yet is markedly elevated in the cells located at the eyelid leading edge (see Fig. 1A). The fact that MAP3K1 expression and activity are localized to the eyelid suprabasal epithelial cells (as shown in Fig. 2B) raises the possibility that MAP3K1 is responsible for c-Jun induction. To test this hypothesis, we examined c-Jun expression in the presence or absence of MAP3K1. At E15, elevated c-Jun was detected in a small cluster of suprabasal cells near the eyelid tip (Fig. 4A). The level of expression was similar in wild type, $Map3k1^{+/\Delta KD}$ and $Map3k1^{\Delta/\Delta KD}$ fetuses, suggesting that c-Jun induction at this stage was independent of MAP3K1 (Figs. 4A and 4B). In contrast, phospho-c-Jun was detected in about 30% of the c-Jun-positive cells in wild type fetuses, and was significantly reduced in $Map3k1^{\Delta/\Delta KD}$ fetuses.

Colchicine is a microtubule depolymerization agent known to activate RhoA, which in turn promotes eyelid closure through the MAP3K1-JNK axis (Danowski, 1989;Enomoto, 1996;Geh et al., 2011;Jung et al., 1997;Nalbant et al., 2009). Using colchicine as a RhoA activating agent, we identified a MAP3K1-dependent induction of JNK and c-Jun phosphorylation in fibroblasts (Fig. 4C) and an increase of filamentous actin, which was slightly potentiated by MAP3K1(WT) but significantly prevented by MAP3K1(KM) in HeLa cells (Fig. 4D). On the other hand, colchicine induced a sustained c-Jun expression in both HeLa cells and fibroblasts, but this event was unaffected by *Map3k1* gene ablation or expression of MAP3K1(WT) or MAP3K1(KM) (Figs. 4C and 4E). Consistent with the findings in the E15 eyelid, *in vitro* responses to colchicine reveal that c-Jun phosphorylation

and actin polymerization are dependent on MAP3K1, but that induction of c-Jun expression is MAP3K1 independent.

In contrast, E15.5 - E16 wild type fetuses, but not *Map3k1*$^{\Delta/\Delta KD}$ fetuses, display strong c-Jun expression in the eyelid tip epithelium (Fig. 4F). Interestingly, c-Jun positive cells were localized in the eyelid protrusion and extension, and these morphological structures were absent in *Map3k1*$^{\Delta/\Delta KD}$ fetuses. Hence, even though MAP3K1 is dispensable for c-Jun induction in the initiation phase, it might, through promotion of eyelid protrusion, cause sustained c-Jun expression in the progressive phase of eyelid closure.

c-Jun is dispensable for MAP3K1 expression and eyelid epithelium protrusion

Our previous *in vitro* data show that c-Jun could bind directly to the *Map3k1* promoter and that MAP3K1 induction by RhoA is abolished by expression of a dominant negative c-Jun or by *c-Jun* gene ablation (Geh et al., 2011). To assess whether c-Jun was required for MAP3K1 expression in the developing eyelids, we crossed *Map3k1*$^{\Delta KD}$ and *Jun*$^{\Delta OSE}$ mice and examined MAP3K1 expression in E15.5 fetuses by X-gal staining. The *Map3k1*$^{+/\Delta KD}$/*Jun*$^{F/F}$ eyelids displayed the same intensity and pattern of X-gal staining regardless of whether *Le-Cre* was present, suggesting that the expression of MAP3K1 *in vivo* was independent of c-Jun (Fig. 5A). In the inferior epithelial cells near the eyelid tip, F-actin content and elongation index were comparable between wild type and *Jun*$^{\Delta/\Delta OSE}$ fetuses, suggesting that the MAP3K1-mediated morphogenetic events were also not affected by c-Jun ablation (Figs. 5B and 5C).

c-Jun and Map3k1 complement each other in eyelid closure

If MAP3K1 and c-Jun were independent of one another in the regulation of eyelid morphogenesis, loss of one allele of each gene should be harmless because the *Map3k1*- and *c-Jun*-hemizygotes had normal eyelid closure. To test this idea, we crossed mice carrying *Map3k1*$^{\Delta KD}$ and *Jun*$^{\Delta OSE}$ alleles and examined eyelid development in the progeny. At E16.5, the size of the eye opening remaining was the same in double hemizygous than in *Map3k1*$^{+/\Delta KD}$ fetuses (n=19), and at birth, all the double hemizygous progeny (*Map3k1*$^{+/\Delta KD}$/*c-Jun*$^{+/F}$/*le-cre*) (n=15) had normal eyelid closure (Figs. 6A and 6B). Hence, *Map3k1* and *c-Jun* complement each other, as double hemizygosity neither blocks nor delays eyelid closure.

DISCUSSION

A powerful genetic tool to delineate the molecular distances between gene products in development and organogenesis is the non-allelic non-complementation test, where recessive mutations in two different loci fail to complement one another and produce a phenotype (Yook et al., 2001). Whereas strong non-complementation occurs among genes encoding products that interact with one another, weak non-complementation could happen among genes whose products do not belong to the same complex but function in the same pathway. In the eyelid closure model, non-complementation occurs between *Map3k1* and *Jnk1, Jnk2* or *RhoA*, whose products physically interact (Gallagher et al., 2002;Gallagher et al., 2003;Geh et al., 2011;Takatori et al., 2008). Several lines of evidence suggest that

MAP3K1 and c-Jun belong to the same pathway. First, MAP3K1 is required for c-Jun phosphorylation in the eyelid epithelium; second, MAP3K1 directly interacts with c-Jun and facilitates its ubiquitylation (Rieger et al., 2012); third, homozygous ablation of either gene produces the EOB phenotype (Li et al., 2003;Zenz et al., 2003;Zhang et al., 2003). Nonetheless, our genetic complementation data show that *c-Jun* and *Map3k1* allelic lesions do not have additive or synergistic effects on preventing eyelid closure. One possible explanation for this phenomenon is that MAP3K1 and c-Jun act on distant points of the same pathway and hence, their interactions are too weak to be detected by the complementation tests. This possibility is supported by the fact that MAP3K1 is a cytosolic protein while c-Jun is located in the nucleus and that these proteins are physically separated. Another possible explanation is that MAP3K1 and c-Jun may regulate two different processes and make distinct contributions to embryonic eyelid closure.

Our biochemical and immunohistochemical data lend support to the second possibility. We show that MAP3K1 and c-Jun play temporal-spatially and mechanistically distinct roles in epithelial cell migration. MAP3K1 is abundantly expressed in inferior epithelial cells of the developing eyelid, where its activity is required for promotion of actin polymerization and elongation of the inferior epithelial cells adjacent to the eyelid leading edge. Promotion of these processes in turn leads to the formation of an epithelium protrusion that marks the initiation of lid closure. c-Jun, on the other hand, is strongly induced in the eyelid leading edge epithelial cells after the initiation of lid closure. Induction of c-Jun is required for ERK phosphorylation and cell migration across the ocular surface. Collective epithelial cell migration involves the coordination of many epithelial cells in space and time and the dynamic changes in cell motility and shape. In the eyelid closure model, epithelial cell migration is coordinated through the consecutive action of MAP3K1, acting at an early phase to initiate epithelium protrusion, and c-Jun, joining in at a later phase to promote forward movement of the epithelium.

An intriguing finding of our work is that significant amount of MAP3K1 is associated with the cytoskeleton and present in the triton-insoluble fraction in many cell types. Although colchicine activates the MAP3K1-JNK cascades (Gibson et al., 1999;Kwan et al., 2001), we find that MAP3K1 is not co-localized with microtubules and that colchicine treatment fails to release it from the Triton-insoluble fraction (Suppl Fig. 2). Quite to the contrary, there is a significant association between MAP3K1 and the actin cytoskeleton in a manner that is independent of its kinase activity. This observation is consistent with a previous report showing that MAP3K1 localizes along F-actin through interaction with the actin-crosslinking protein α-actinin (Christerson et al., 1999). This physical association is postulated to restrict MAP3K1 to the actin cytoskeleton where it would regulate specific downstream targets. Accordingly, we find that MAP3K1 activity potentiates F-actin and stress fiber formation *in vitro* and *in vivo*. This function may involve JNK, as JNK is shown to cooperate with MAP3K1 for eyelid closure, and directly modulate F-actin organization in fruit flies and mammalian cells (Fernandez et al., 2013;Huang et al., 2003;Takatori et al., 2008).

The *Map3k1* promoter has multiple AP-1-binding sites and its induction is causally related to that of c-Jun; however, c-Jun is neither essential nor sufficient for the induction of

MAP3K1. Conversely, the expression of c-Jun is barely detectable in embryonic epidermis, but is robustly induced in the epithelial cells of the eyelid leading edge (Li et al., 2003;Zenz et al., 2003). MAP3K1 is not involved in c-Jun induction at the initiation phase of eyelid closure. This is consistent with our previous global gene expression data showing that MAP3K1 ablation does not affect the expression of c-Jun or of c-Jun/AP-1 target genes (Jin et al., 2012).

The leading edge epithelial cell elongation, apical actin-cable formation and cell intercalation are the driving force for epithelial sheet movement in eyelid closure (Grose, 2003;Heller et al., 2014;Thumkeo et al., 2005). These processes may depend on c-Jun, as c-Jun is not only strongly expressed in the leading edge cells, but also involved in the potentiation of ERK phosphorylation and expression of migration markers in the eyelid tip cells. The nature of the direct c-Jun targets in this event is yet to be uncovered, but we may speculate as to their identity based on data from mice in which *JunB* was knocked-in at the *c-Jun* locus (Passegue et al., 2002). In these mice, JunB replaces c-Jun in liver and heart development, but does not rescue the eyelid closure defects. Since JunB restores the expression of genes regulated by Jun/Fos, but not those regulated by Jun/ATF, it is reasonable to conclude that genes involved in eyelid closure are targets of the c-Jun/ATF complexes, which have been shown to preferentially regulate promoters containing a single AP-1-binding site (van and Castellazzi, 2001). Indeed, several putative c-Jun target genes known to be involved in eyelid closure, such as *Hb-egf, Tgf*α, *Egfr* and *Itga5*, have a functional AP-1 element in their promoters (Johnson et al., 2000;Li et al., 2003;Luetteke and Lee, 1990;Park et al., 1999;Qin et al., 2011;Raab and Klagsbrun, 1997;Zenz et al., 2003).

In the present work, we describe a scenario where MAP3K1-mediated actin assembly in inferior epithelial cells occurs prior to c-Jun-mediated leading edge cell migration and the temporal-spatially distinct pathways and cellular activities both contribute to embryonic eyelid closure. Among the numerous morphogenetic pathways proven to be crucial for eyelid closure, the EGFR and integrin signaling is activated in the leading edge, whereas the BMP and Wnt signaling appears to be effective in the inferior epithelial cells (Grose, 2003;Heller et al., 2014;Huang et al., 2009;Wu et al., 2012). Collaboration of the various signaling pathways in different while adjacent regions may be a prominent mechanism for the concerted epithelial sheet movement. Understanding these regulatory pathways in eyelid closure may shed new light into mechanisms of wound healing and tumor metastasis, in which epithelial cell migration also plays a pivotal role.

Supplementary Material

Refer to Web version on PubMed Central for supplementary material.

Acknowledgments

We wish to thank Drs. Randall Johnson for *c-Jun*^{F} mice and Alvaro Puga (University of Cincinnati) for a critical reading of the manuscript. The work is supported in part by funding from NIH, NEI R01-EY15227 (Y.X.).

REFERENCES

Behrens A, Sibilia M, Wagner EF. Amino-terminal phosphorylation of c-Jun regulates stress-induced apoptosis and cellular proliferation. Nat. Genet. 1999; 21:326–329. [PubMed: 10080190]

Christerson LB, Vanderbilt CA, Cobb MH. MEKK1 interacts with alpha-actinin and localizes to stress fibers and focal adhesions. Cell Motil Cytoskeleton. 1999; 43:186–98. [PubMed: 10401575]

Danowski BA. Fibroblast contractility and actin organization are stimulated by microtubule inhibitors. J. Cell Sci. 1989; 93(Pt 2):255–266. [PubMed: 2482296]

Deng M, Chen WL, Takatori A, Peng Z, Zhang L, Mongan M, Parthasarathy R, Sartor M, Miller M, Yang J, Su B, Kao WW, Xia Y. A role for the mitogen-activated protein kinase kinase kinase 1 in epithelial wound healing. Mol. Biol. Cell. 2006; 17:3446–3455. [PubMed: 16760432]

Derijard B, Hibi M, Wu IH, Barrett T, Su B, Deng T, Karin M, Davis RJ. JNK1: a protein kinase stimulated by UV light and Ha-Ras that binds and phosphorylates the c-Jun activation domain. Cell. 1994; 76:1025–1037. [PubMed: 8137421]

Enomoto T. Microtubule disruption induces the formation of actin stress fibers and focal adhesions in cultured cells: possible involvement of the rho signal cascade. Cell Struct. Funct. 1996; 21:317–326. [PubMed: 9118237]

Fernandez BG, Jezowska B, Janody F. Drosophila actin-Capping Protein limits JNK activation by the Src proto-oncogene. Oncogene. 2013

Findlater GS, McDougall RD, Kaufman MH. Eyelid development, fusion and subsequent reopening in the mouse. J Anat. 1993; 183:121–9. [PubMed: 8270467]

Fowler KJ, Walker F, Alexander W, Hibbs ML, Nice EC, Bohmer RM, Mann GB, Thumwood C, Maglitto R, Danks JA. A mutation in the epidermal growth factor receptor in waved-2 mice has a profound effect on receptor biochemistry that results in impaired lactation. Proc. Natl. Acad. Sci. U. S. A. 1995; 92:1465–1469. [PubMed: 7533293]

Gallagher ED, Gutowski S, Sternweis PC, Cobb MH. RhoA binds to the amino-terminus of MEKK1 and regulates its kinase activity. J. Biol. Chem. 2003

Gallagher ED, Xu S, Moomaw C, Slaughter CA, Cobb MH. Binding of JNK/SAPK to MEKK1 is regulated by phosphorylation. J. Biol. Chem. 2002; 277:45785–45792. [PubMed: 12228228]

Geh E, Meng Q, Mongan M, Wang J, Takatori A, Zheng Y, Puga A, Lang RA, Xia Y. Mitogen-activated protein kinase kinase kinase 1 (MAP3K1) integrates developmental signals for eyelid closure. Proc. Natl. Acad. Sci. U. S. A. 2011; 108:17349–17354. [PubMed: 21969564]

Gibson S, Widmann C, Johnson GL. Differential involvement of MEK kinase 1 (MEKK1) in the induction of apoptosis in response to microtubule-targeted drugs versus DNA damaging agents. J Biol Chem. 1999; 274:10916–22. [PubMed: 10196170]

Grose R. Epithelial migration: open your eyes to c-Jun. Curr. Biol. 2003; 13:R678–R680. [PubMed: 12956972]

Gumbiner BM. Epithelial morphogenesis. Cell. 1992; 69:385–387. [PubMed: 1581959]

Harris MJ, McLeod MJ. Eyelid growth and fusion in fetal mice. A scanning electron microscope study. Anat. Embryol.(Berl). 1982; 164:207–220. [PubMed: 7125235]

Hassemer EL, Le Gall SM, Liegel R, McNally M, Chang B, Zeiss CJ, Dubielzig RD, Horiuchi K, Kimura T, Okada Y, Blobel CP, Sidjanin DJ. The waved with open eyelids (woe) locus is a hypomorphic mouse mutation in Adam17. Genetics. 2010; 185:245–255. [PubMed: 20194968]

Heller E, Kumar KV, Grill SW, Fuchs E. Forces generated by cell intercalation tow epidermal sheets in Mammalian tissue morphogenesis. Dev. Cell. 2014; 28:617–632. [PubMed: 24697897]

Hibi M, Lin A, Smeal T, Minden A, Karin M. Identification of an oncoprotein- and UV-responsive protein kinase that binds and potentiates the c-Jun activation domain. Genes Dev. 1993; 7:2135–48. [PubMed: 8224842]

Huang C, Rajfur Z, Borchers C, Schaller MD, Jacobson K. JNK phosphorylates paxillin and regulates cell migration. Nature. 2003; 424:219–223. [PubMed: 12853963]

Huang J, Dattilo LK, Rajagopal R, Liu Y, Kaartinen V, Mishina Y, Deng CX, Umans L, Zwijsen A, Roberts AB, Beebe DC. FGF-regulated BMP signaling is required for eyelid closure and to specify conjunctival epithelial cell fate. Development. 2009; 136:1741–1750. [PubMed: 19369394]

Jin C, Chen J, Meng Q, Carreira V, Tam NN, Geh E, Karyala S, Ho SM, Zhou X, Medvedovic M, Xia Y. Deciphering gene expression program of MAP3K1 in mouse eyelid morphogenesis. Dev. Biol. 2012

Johnson AC, Murphy BA, Matelis CM, Rubinstein Y, Piebenga EC, Akers LM, Neta G, Vinson C, Birrer M. Activator protein-1 mediates induced but not basal epidermal growth factor receptor gene expression. Mol Med. 2000; 6:17–27. [PubMed: 10803405]

Jung HI, Shin I, Park YM, Kang KW, Ha KS. Colchicine activates actin polymerization by microtubule depolymerization. Mol Cells. 1997; 7:431–7. [PubMed: 9264034]

Kwan R, Burnside J, Kurosaki T, Cheng G. MEKK1 is essential for DT40 cell apoptosis in response to microtubule disruption. Mol. Cell Biol. 2001; 21:7183–7190. [PubMed: 11585901]

Li G, Gustafson-Brown C, Hanks SK, Nason K, Arbeit JM, Pogliano K, Wisdom RM, Johnson RS. c-Jun Is Essential for Organization of the Epidermal Leading Edge. Dev. Cell. 2003; 4:865–877. [PubMed: 12791271]

Luetteke NC, Lee DC. Transforming growth factor alpha: expression, regulation and biological action of its integral membrane precursor. Semin. Cancer Biol. 1990; 1:265–275. [PubMed: 2103501]

Miettinen PJ, Berger JE, Meneses J, Phung Y, Pedersen RA, Werb Z, Derynck R. Epithelial immaturity and multiorgan failure in mice lacking epidermal growth factor receptor. Nature. 1995; 376:337–41. [PubMed: 7630400]

Mine N, Iwamoto R, Mekada E. HB-EGF promotes epithelial cell migration in eyelid development. Development. 2005; 132:4317–4326. [PubMed: 16141218]

Mohamed YH, Gong H, Amemiya T. Role of apoptosis in eyelid development. Exp. Eye Res. 2003; 76:115–123. [PubMed: 12589781]

Mongan M, Tan Z, Chen L, Peng Z, Dietsch M, Su B, Leikauf G, Xia Y. Mitogen-activated protein kinase kinase kinase 1 protects against nickel-induced acute lung injury. Toxicol. Sci. 2008; 104:405–411. [PubMed: 18467339]

Nalbant P, Chang YC, Birkenfeld J, Chang ZF, Bokoch GM. Guanine nucleotide exchange factor-H1 regulates cell migration via localized activation of RhoA at the leading edge. Mol. Biol. Cell. 2009; 20:4070–4082. [PubMed: 19625450]

Park JM, Adam RM, Peters CA, Guthrie PD, Sun Z, Klagsbrun M, Freeman MR. AP-1 mediates stretch-induced expression of HB-EGF in bladder smooth muscle cells. Am. J. Physiol. 1999; 277:C294–C301. [PubMed: 10444406]

Passegue E, Jochum W, Behrens A, Ricci R, Wagner EF. JunB can substitute for Jun in mouse development and cell proliferation. Nat. Genet. 2002; 30:158–166. [PubMed: 11818961]

Posern G, Miralles F, Guettler S, Treisman R. Mutant actins that stabilise F-actin use distinct mechanisms to activate the SRF coactivator MAL. EMBO J. 2004; 23:3973–3983. [PubMed: 15385960]

Qin L, Chen X, Wu Y, Feng Z, He T, Wang L, Liao L, Xu J. Steroid receptor coactivator-1 upregulates integrin alpha(5) expression to promote breast cancer cell adhesion and migration. Cancer Res. 2011; 71:1742–1751. [PubMed: 21343398]

Raab G, Klagsbrun M. Heparin-binding EGF-like growth factor. Biochim. Biophys. Acta. 1997; 1333:F179–F199. [PubMed: 9426203]

Rieger MA, Duellman T, Hooper C, Ameka M, Bakowska JC, Cuevas BD. The MEKK1 SWIM domain is a novel substrate receptor for c-Jun ubiquitylation. Biochem. J. 2012; 445:431–439. [PubMed: 22582703]

Schnekenburger M, Peng L, Puga A. HDAC1 bound to the Cyp1a1 promoter blocks histone acetylation associated with Ah receptor-mediated trans-activation. Biochim. Biophys. Acta. 2007; 1769:569–578. [PubMed: 17707923]

shery-Padan R, Marquardt T, Zhou X, Gruss P. Pax6 activity in the lens primordium is required for lens formation and for correct placement of a single retina in the eye. Genes Dev. 2000; 14:2701–2711. [PubMed: 11069887]

Sibilia M, Wagner EF. Strain-dependent epithelial defects in mice lacking the EGF receptor. Science. 1995; 269:234–8. [PubMed: 7618085]

Takatori A, Geh E, Chen L, Zhang L, Meller J, Xia Y. Differential transmission of MEKK1 morphogenetic signals by JNK1 and JNK2. Development. 2008; 135:23–32. [PubMed: 18032450]

Threadgill DW, Dlugosz AA, Hansen LA, Tennenbaum T, Lichti U, Yee D, LaMantia C, Mourton T, Herrup K, Harris RC, et al. Targeted disruption of mouse EGF receptor: effect of genetic background on mutant phenotype. Science. 1995; 269:230–4. [PubMed: 7618084]

Thumkeo D, Shimizu Y, Sakamoto S, Yamada S, Narumiya S. ROCK-I and ROCK-II cooperatively regulate closure of eyelid and ventral body wall in mouse embryo. Genes Cells. 2005; 10:825–834. [PubMed: 16098146]

Uhlik MT, Abell AN, Cuevas BD, Nakamura K, Johnson GL. Wiring diagrams of MAPK regulation by MEKK1, 2, and 3. Biochem. Cell Biol. 2004; 82:658–663. [PubMed: 15674433]

van DH, Castellazzi M. Distinct roles of Jun: Fos and Jun: ATF dimers in oncogenesis. Oncogene. 2001; 20:2453–2464. [PubMed: 11402340]

Weston CR, Wong A, Hall JP, Goad ME, Flavell RA, Davis RJ. JNK initiates a cytokine cascade that causes Pax2 expression and closure of the optic fissure. Genes Dev. 2003; 17:1271–1280. [PubMed: 12756228]

Wu CI, Hoffman JA, Shy BR, Ford EM, Fuchs E, Nguyen H, Merrill BJ. Function of Wnt/beta-catenin in counteracting Tcf3 repression through the Tcf3-beta-catenin interaction. Development. 2012; 139:2118–2129. [PubMed: 22573616]

Xia Y, Makris C, Su B, Li E, Yang J, Nemerow GR, Karin M. MEK kinase 1 is critically required for c-Jun N-terminal kinase activation by proinflammatory stimuli and growth factor-induced cell migration. Proc Natl Acad Sci U S A. 2000; 97:5243–8. [PubMed: 10805784]

Yook KJ, Proulx SR, Jorgensen EM. Rules of nonallelic noncomplementation at the synapse in Caenorhabditis elegans. Genetics. 2001; 158:209–220. [PubMed: 11333231]

Yujiri T, Sather S, Fanger GR, Johnson GL. Role of MEKK1 in cell survival and activation of JNK and ERK pathways defined by targeted gene disruption. Science. 1998; 282:1911–4. [PubMed: 9836645]

Zenz R, Scheuch H, Martin P, Frank C, Eferl R, Kenner L, Sibilia M, Wagner EF. c-Jun Regulates Eyelid Closure and Skin Tumor Development through EGFR Signaling. Dev. Cell. 2003; 4:879–889. [PubMed: 12791272]

Zhang L, Wang W, Hayashi Y, Jester JV, Birk DE, Gao M, Liu CY, Kao WW, Karin M, Xia Y. A role for MEK kinase 1 in TGF-beta/activin-induced epithelium movement and embryonic eyelid closure. Embo J. 2003; 22:4443–4454. [PubMed: 12941696]

Highlights

- loss of c-Jun and MAP3K1 result in defective eyelid closure in embryogenesis
- MAP3K1 promotes actin polymerization and initiation of eyelid closure
- c-Jun is effective after the eyelid closure process is initiated
- MAP3K1 and c-Jun are independent of each other for expression
- c-Jun and MAP3K1 represent parallel pathways in the control of eyelid closure

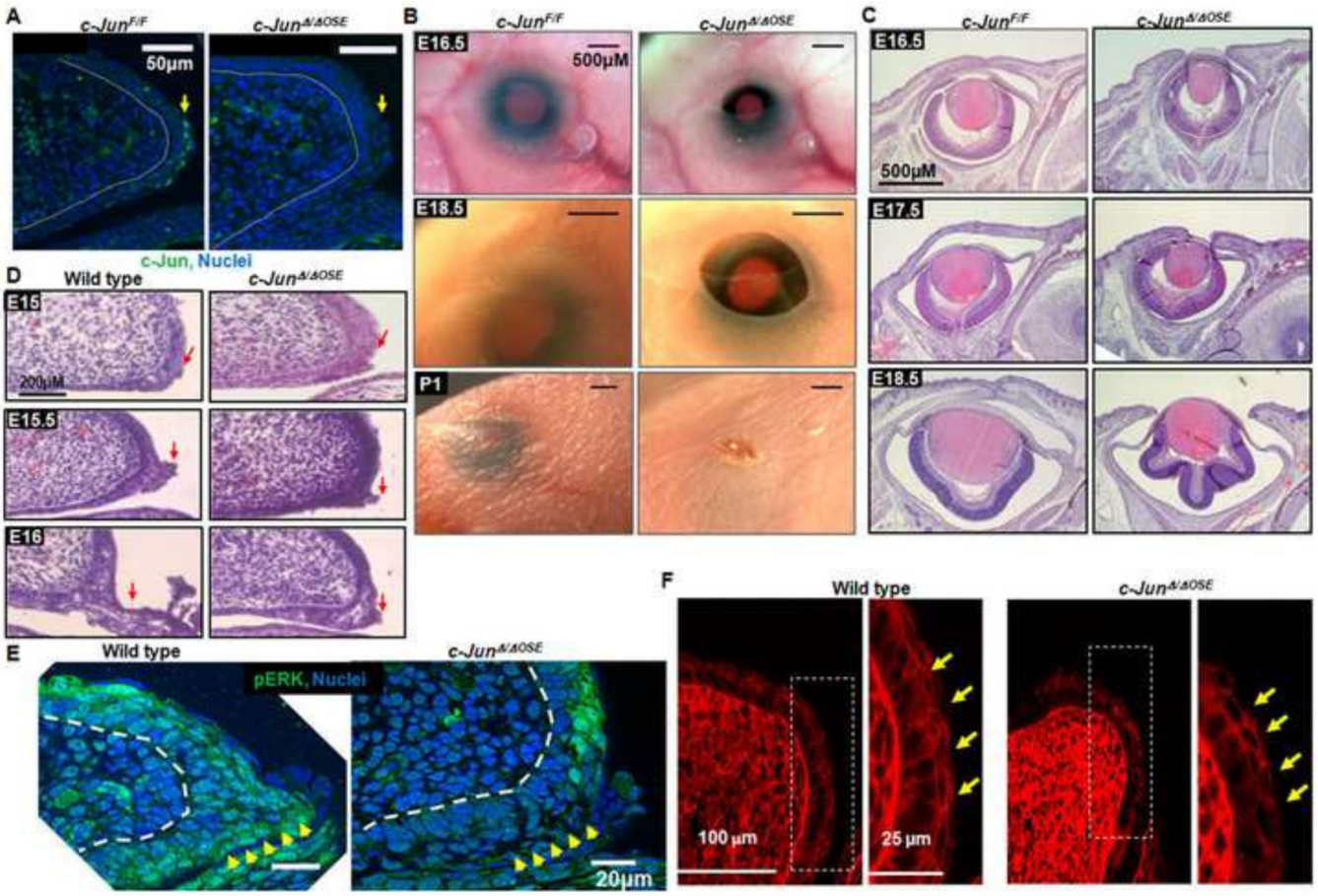

Figure 1. c-Jun expression is essential for epithelial cell migration and eyelid closure

(A) The E15 eyelid was examined for c-Jun (green) and F-actin (red). While strong c-Jun expression was detected in epithelial cells at the eyelid tip of *c-Jun*$^{F/F}$, it was absent in that of *c-Jun*$^{\Delta/\Delta OSE}$ fetuses. Eyes of *c-Jun*$^{F/F}$ and *c-Jun*$^{\Delta/\Delta OSE}$ fetuses/mice (B) at E16.5 to P1 were photographed, and (C) at E16.5 to E18.5 were examined by histology. Failure of eyelid closure was detected in the *c-Jun*$^{\Delta/\Delta OSE}$ mice. (D) Histology of E15 to E16 eyes, represented pre-initiation (E15), initiation (E15.5) and progression (E16) phases of embryonic eyelid closure. Immunohistochemistry of *c-Jun*$^{F/F}$ and *c-Jun*$^{\Delta/\Delta OSE}$ E15.5 eyes using (E) anti-pERK (green) with the arrowheads pointing at the p-ERK positive cells, and (F) anti-β-catenin (red), with photographs taken at low (left panels) and high (right panels) magnifications. The arrows point at the eyelid leading edge and dotted lines mark basement membrane.

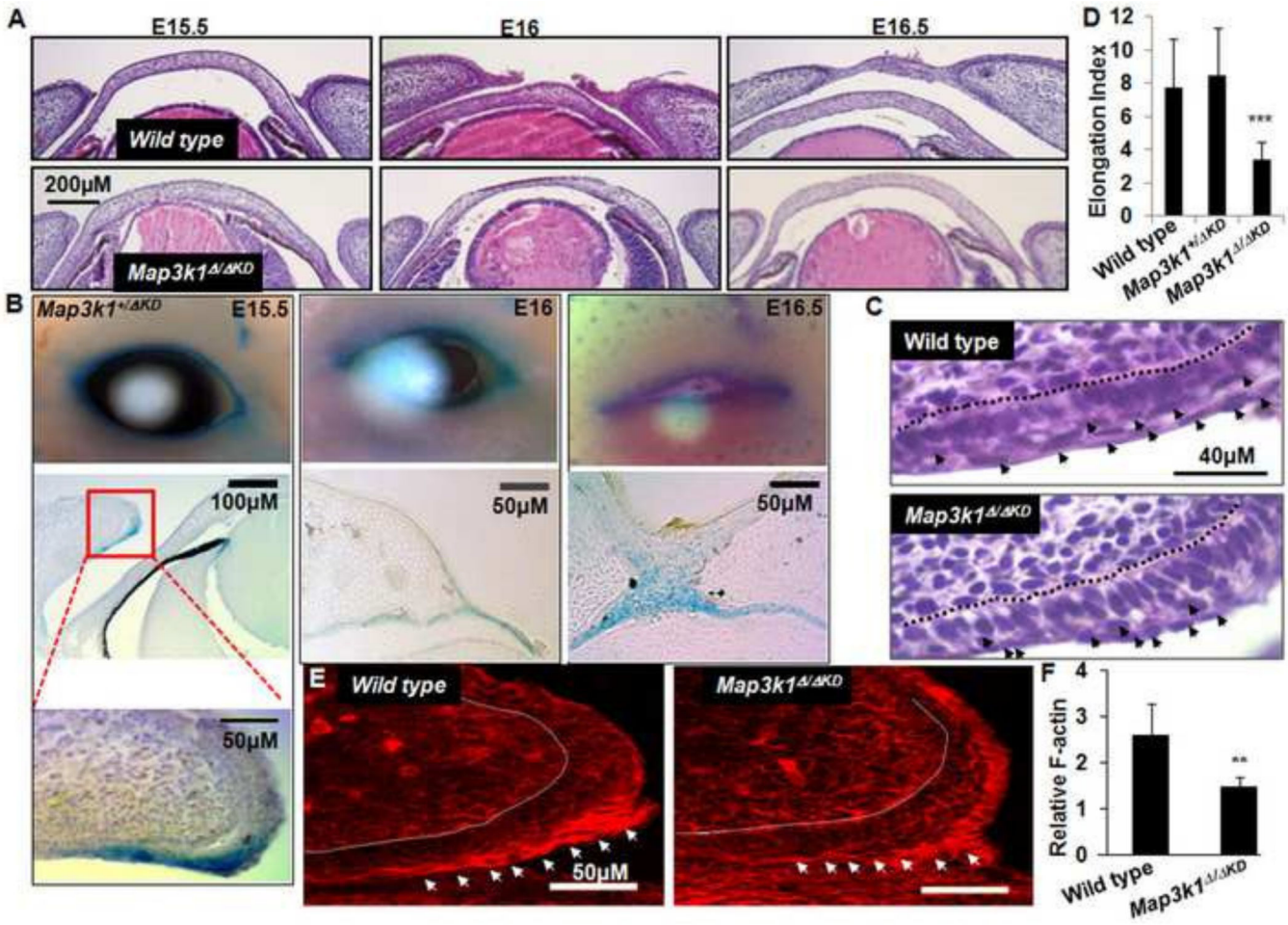

Figure 2. MAP3K1 is required for actin polymerization and epithelial cell elongation

(A) Histology of wild type and *Map3k1*$^{\Delta/\Delta KD}$ eyes at the initiation (E15.5), progression (E16), and completion (E16.5) phases of embryonic eyelid closure. (B) Whole-mount X-gal staining of the *Map3k1*$^{+/\Delta KD}$ fetuses at E15.5 - E16.5. Photographs were taken of the eyes (upper panels) or of the eye sections counter-stained with hematoxyline (purple) (middle and lower panels). The β-gal positive cells (light blue) were abundant in inferior eyelid epithelium and in epithelial cells near the eyelid tip. (C) Histology or (E) Alexa-fluor (594)-conjugated phalloidin staining of wild type and *Map3k1*$^{\Delta/\Delta KD}$ E15.5 eyelids. Arrows point at (C) the elongated epithelial cells and (E) cells with increased F-actin in wild type and corresponding cells lacking thereof in *Map3k1*$^{\Delta/\Delta KD}$ fetuses. Of these cells, (D) the elongation index and (F) relative F-actin intensity were calculated. Total of 18 eyelids of each genotype were examined. **p<0.01 and ***p<0.001 were considered statistically significant. The dotted lines mark basement membrane.

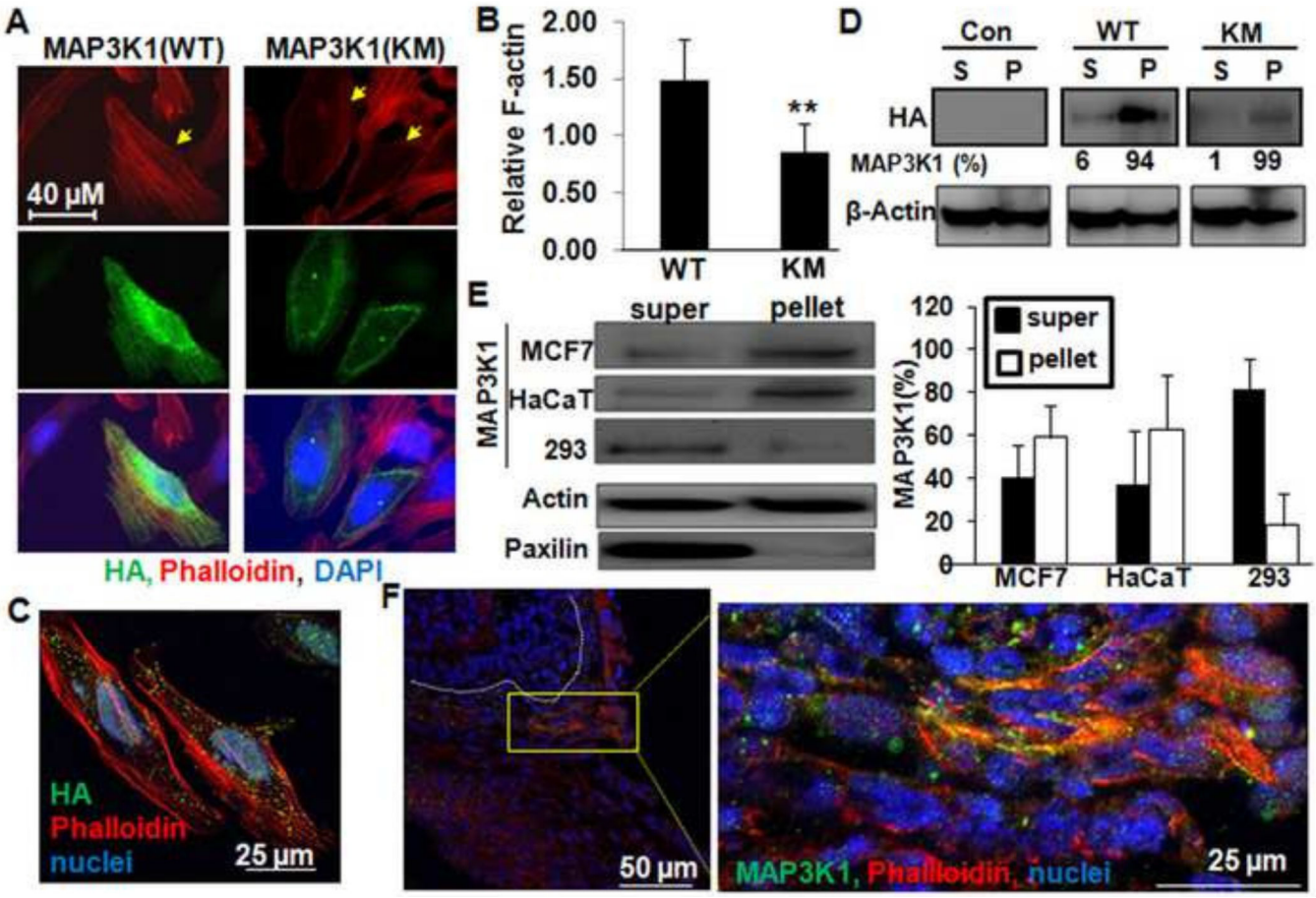

Figure 3. MAP3K1 is physically associated with cytoskeleton and colocalized to F-actin

HeLa cells transfected with mammalian expression vectors for HA-MAP3K1 or HA-MAP3K1-KM were stained with anti-HA (green), phalloidin (red) and DAPI (blue). The transfection efficiency was estimated to be 10 % and 15 % for MAP3K1(WT) and MAP3K1(KM), respectively. Photographs were taken using (A) a plan fluorescence or (C) a laser scanning microscope. (B) The relative F-actin intensity was calculated by comparing the phalloidin (red) signal/cell area among HA (green) positive versus HA negative cells in each set of transfections. Results are average values of 3 independent experiments with at least fifty cells in randomly selected fields and 3 fields/experiments. (D) The HEK 293 cells transfected with either empty vector or expression vectors for HA-MAP3K1 and HA-MAP3K1-KM, or (E) the un-transfected HEK 293, HaCaT and MCF7 cells were lysed and prepared for triton-soluble (s) and triton-insoluble (p) fractions. The fractions were subjected to Western blotting using (D) anti-HA and (E) anti-MAP3K1 and anti-paxillin, and anti-β-Actin served as a loading control. The percentage of MAP3K1 proteins in each fraction was calculated by comparing the IB signals in each fraction to the sum (s+p). (F) The eyes of wild type E15.5 fetuses were subjected to immunostaining with anti-MAP3K1 (green), together with phalloidin (red) and DAPI (blue). Photographs were taken using a laser scanning microscope. The dotted lines mark basement membrane.

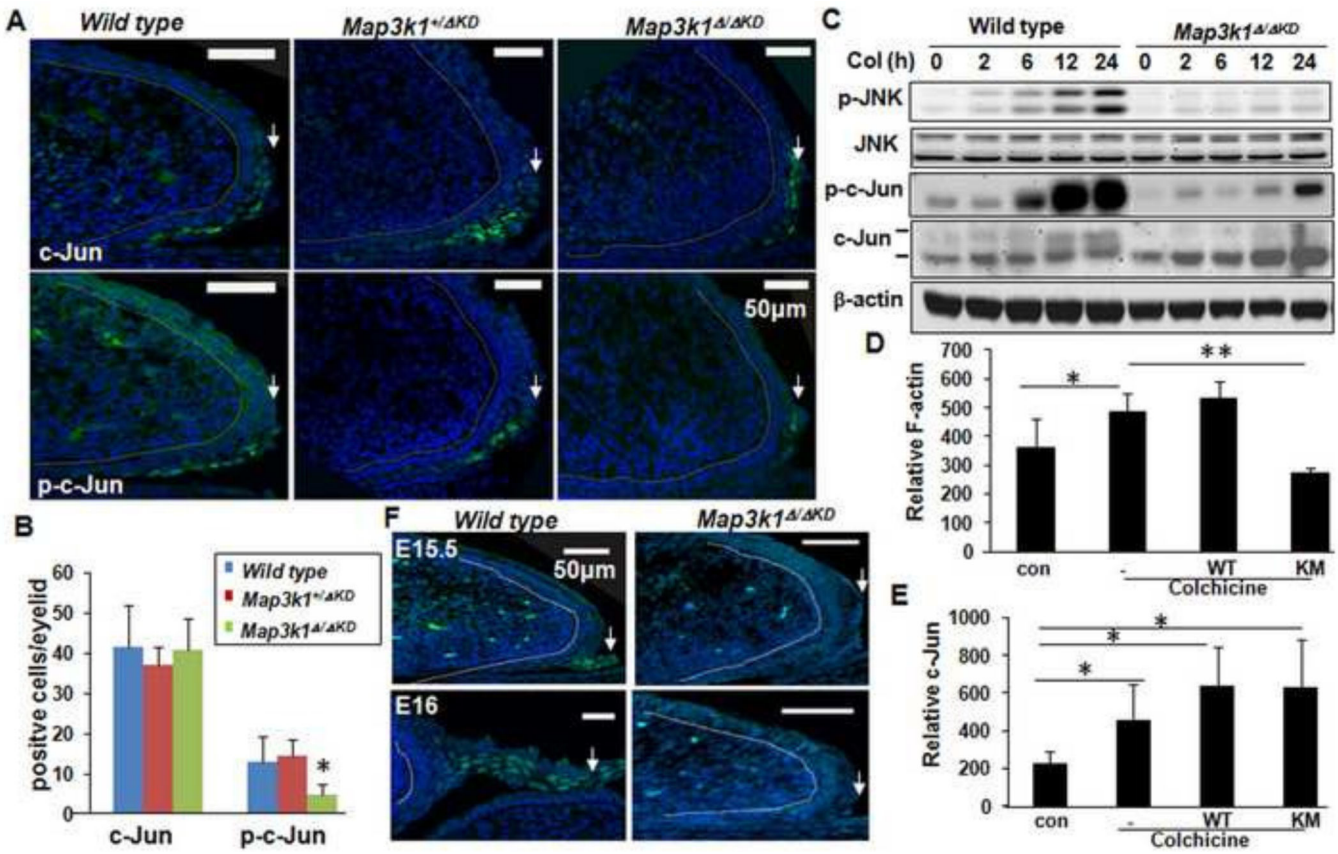

Figure 4. MAP3K1 is required for c-Jun phosphorylation, but not c-Jun expression

(A) Immunostaining for c-Jun (upper panels) and p-c-Jun (green, lower panels) in E15 wild type, *Map3k1*$^{+/\Delta KD}$ and *Map3k1*$^{\Delta/\Delta KD}$ eyelids. Positive cells were identified in epithelium at the eyelid leading edge (arrows). (B) Quantification of c-Jun and p-c-Jun positive cells in the eyelids. (C) Wild type and *Map3k1*$^{\Delta/\Delta KD}$ fibroblasts were treated with 1μM colchicine for various times; cell lysates were subjected to Western blotting with the indicated antibodies. HeLa cells transfected with either an empty vector or expression vectors for HA-MAP3K1 and HA-MAP3K1-KM were treated or not with 5 μM colchicine for 6 h, followed by fixation and fluorescence staining using anti-HA, in conjunction with (D) phalloidin or (E) anti-c-Jun. The average intensity of fluorescence signal for (D) F-actin and (E) c-Jun/cell area were quantified, and compared to those in HA-negative cells without colchicine treatment. (F) c-Jun immunostaining (green) of E16 wild type and *Map3k1*$^{\Delta KD/\Delta KD}$ fetuses. DAPI (blue) were used to label nuclei. Arrows point at eyelid leading edge and dotted lines mark basement membrane. *p<0.05, and **p<0.01 indicate values significantly different from the control.

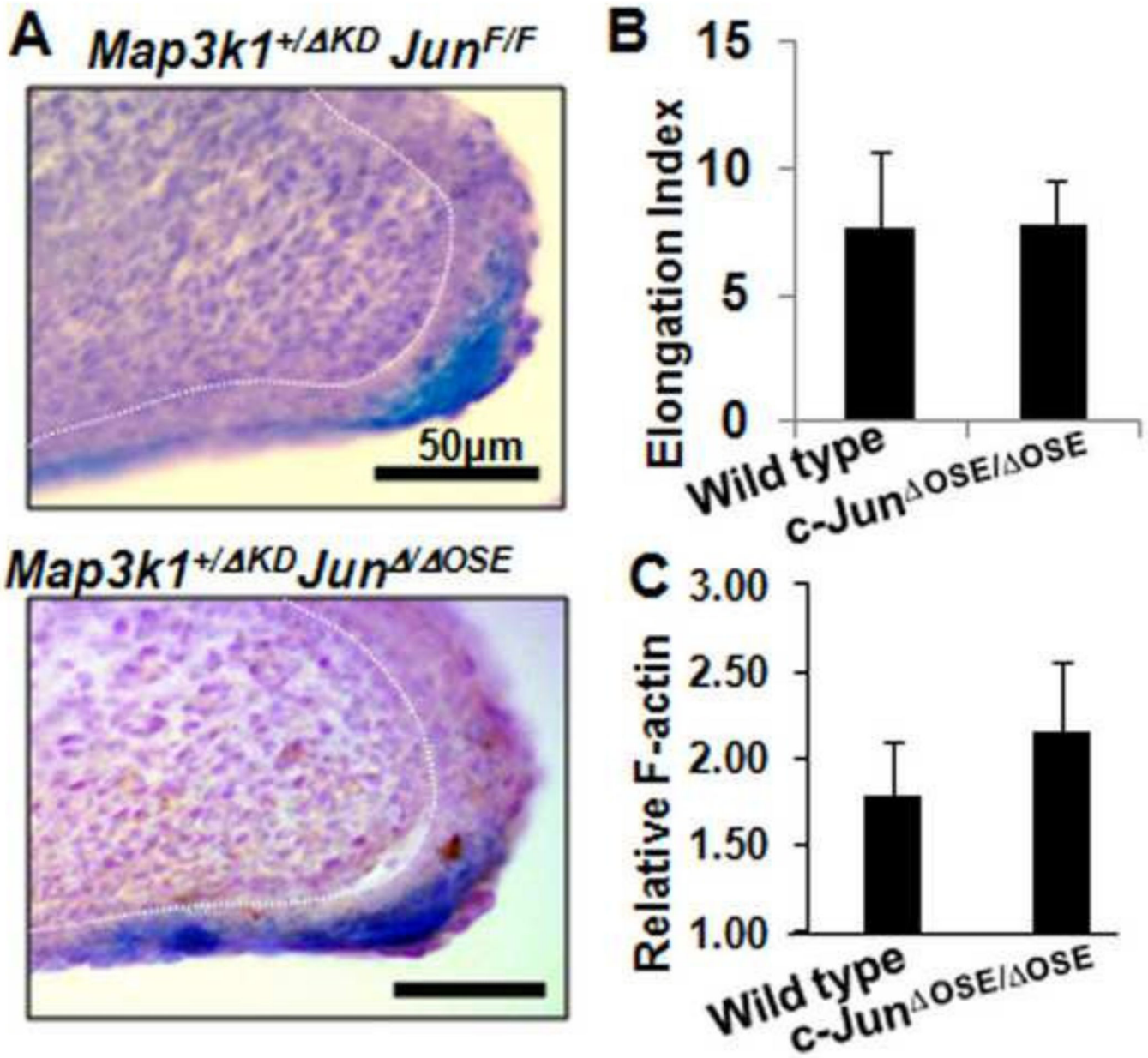

Figure 5. c-Jun is dispensable for MAP3K1 expression

(A) The E15 *Map3k1*$^{+/\Delta KD}$/*c-Jun*$^{F/F}$ and *Map3k1*$^{+/\Delta KD}$/*c-Jun*$^{\Delta/\Delta OSE}$ fetuses were subjected to whole mount X-gal staining (dark blue). The eye histology sections were counter-stained with hematoxylin (purple). Dotted lines mark the borders of the basement membrane. A cluster of β-gal positive cells was identified located at the eyelid inferior epithelium near the leading edge regardless of the genotype. (B) The elongation index and (C) F-actin contents after Alexa-phalloidin staining in inferior epithelial cells near the eyelid tip in *c-Jun*$^{F/F}$ and *c-Jun*$^{\Delta/\Delta OSE}$ E15.5 fetuses. Results represented the average of 2 sections/eye and 4 eyes/genotype examined.

Figure 6. Lack of genetic crosstalk between *c-Jun* and *Map3k1* in embryonic eyelid closure

(A) The *Map3k1*$^{+/\Delta KD}$/*c-Jun*$^{+/F}$ and *Map3k1*$^{+/\Delta KD}$/*c-Jun*$^{+/\Delta OSE}$ fetuses at E16.5 were collected and the eyes were photographed. (B) The sizes of eye opening were measured in a total of 19 fetuses. The average opening sizes in the *Map3k1*$^{+/\Delta KD}$/*c-Jun*$^{+/F}$ fetuses were not significantly different in the presence or absence of *Le-Cre*.